Detection of Rail Defects Using Phased Array Ultrasonic Technique

Nichapa Phrommahakul [1], *Manwika* Kongpuang[1,2*], *Suhaidee* Sani[3], *Anas* Katib[1], and *Fittriya* Sulong[1]

[1]Department of Mining and Materials Engineering, Faculty of Engineering, Prince of Songkla University, Hat Yai, Songkhla, 90110, Thailand
[2]Center of Excellence in Metal and Materials Engineering, Faculty of Engineering, Prince of Songkla University, Hat Yai, Songkhla, 90110, Thailand
[3]Department of Industrial Engineering, Rajamangala University of Technology Srivijaya, Muang, Songkhla 90000, Thailand

Abstract. The Phased Array Ultrasonic Technique (PAUT) is an advanced non-destructive inspection method that utilizes an array of ultrasonic testing (UT) probes consisting of several small elements. The laboratory used an artificial crack on the rail steel grade 900A/ R260 test block to study the principles of PAUT and how to measure the defect's reliability and accuracy. On-site studies were done on railroad tracks with different structures. Rail steel grade 900A/ R260, Hadfield steel, and thermite welded joints. No defects were found during the inspection at the crossing nose of the two positions. Only a darker shade of color in the area has an impact load from the wheel applied when a train changes to another direction. Inspection was also performed for the Thermit welded rail joint with two position defects. The inspection results found defects such as porosity, with an echo (A%) value exceeding 80%, but it does not require rejection according to the BART standard.

1 Introduction

An additional objective of the railway development project is to establish Thailand as the primary transportation center of the area, following the 20-year plan outlined in the National Strategy. When trains are used more frequently, damage will inevitably occur. Therefore, inspections must be carried out to prevent damage. Currently, there are several methods to inspect the rail tracks. Even if the application of radiography for the inspection of austenitic cast manganese in the field was straightforward, the presence of internal cracks could be easily missed due to the limitations of this technique in detecting small cracks. Eddy current testing can detect surface and near-surface defects but remains extremely sensitive to lift-off variations [1-2]. Ultrasonic testing methods are the most popular among NDT used for rail tracks, but they still suffer from high levels of attenuation of the interrogating ultrasonic beam, and therefore, inspection remains unreliable at best [3]. However, such inspection often has problems when inspecting areas with large or coarse structures, such as austenitic grain structure at the crossing nose and cast structure at the weld line [4].

PAUT, an advanced Non-destructive Technique, offers several advantages over conventional ultrasonic testing. It reduces the number of probes and labor needed for inspection, increasing job efficiency. Moreover, due to the electronic control of the angle range, phased-array testing encompasses a broader region, enhancing the coverage and minimizing the chances of missed detections [5]. PAUT, with its unique electronic scanning capability, may efficiently substitute manual grid scans and enhance efficiency. PAUT allows for flexible adjustment of the scanning angle, resulting in a significant improvement in testing efficiency. The PAUT technique is employed to assess the effectiveness of fault identification in rail welds using pneumatic welding.

Additionally, a position marking scale is developed for phased array testing of rail welds to efficiently establish the scanning location of the probe [6-7]. By extending the inspection amount, the physical motion of the phased array probe is significantly reduced, resulting in shorter results and scanning time. These save costs in terms of labor, radiation exposure, and critical path time.

The researcher divided the test into two parts. Those were tested in the laboratory and field. Both parts were tested using an OmniScan™ X3 64 Phased Array and TFM Flaw Detector with Advanced Capabilities.

2 Materials and Methods

2.1 High Manganese steel

The microstructure of high manganese steel or Hadfield steel consists of an austenite-grain matrix containing 11-15 in wt % Mn, with 0.8-1.25 in wt % C [8] with dispersed carbide precipitates, also present mainly at the austenite grain boundaries. The carbides present result in reduced ductility, leading to cracking along the grain boundary (intergranular cracking) (Fig. 1(a)). Hadfield steel is

*Corresponding author : manwika.k@psu.ac.th

capable of being work-hardened very rapidly. When the maximum hardness is reached, it will become the crack path [4]. Therefore, inspection must be done regularly.

2.2 R260 rail steel

R260 rail steel has a fully pearlitic structure with a fine grain containing 0.78 in wt % C and 0.75 in wt % Mn [4]. R260 has an alternating α-ferrite and cementite (Fe_3C) layers arranged in lamellar formations (Fig. 1(b)). R260 is hot-rolled, resulting in free-form defects. It has an initial hardness of 260 HBN (equivalent to 275 HV). The work-hardening rate of ferrite-pearlite steel increases linearly with the increase in the quantity of pearlite in the matrix [12].

2.3 Thermite weld rail joint

Thermit welding has become a widely used welding technique, with fusion and pressure techniques. The chemical reaction of iron-oxide is reduced to pure iron by aluminum, accompanied by heat generation, while aluminum-oxide forms [9]. As equations (1)-(3) indicate, a chemical reaction will occur. Aluminum is reduced to get pure iron, which releases heat and simultaneously forms aluminum oxide.
The structure welded by Thermit is pearlitic, as shown in Fig. 3(c). It is a hypoeutectoid alloy structure with a carbon content of approximately 0.56 wt %. A pearlitic structure surrounds Fe_3C and has the characteristics of network carbides. The effect on the properties of Thermit welded is that it is hard and brittle, resulting in low strength, which may cause damage. Inspecting thermite welds has always been a difficult one in the rail industry. In addition to metallurgical changes, defects that develop from these welds typically arise in areas where it is challenging to introduce any energy for a thorough inspection [10].

Thermite chemical reaction:

$$3\,FeO + 2\,Al = 3\,Fe + Al_2O_3 + 697\,kJ \quad (1)$$
$$Fe_2O_3 + 2Al = 2\,Fe + Al_2O_3 + 831\,kJ \quad (2)$$
$$3\,Fe_3O_4 + 2\,Al = 9\,Fe + 4\,Al_2O_3 + 782\,kJ \quad (3)$$

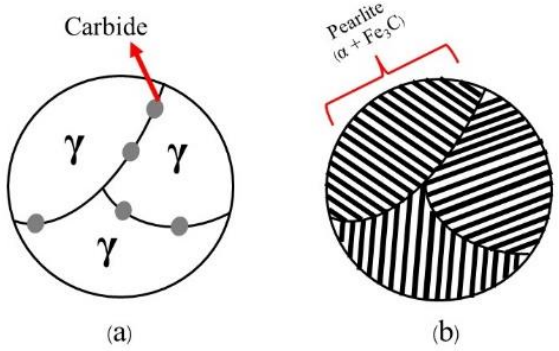

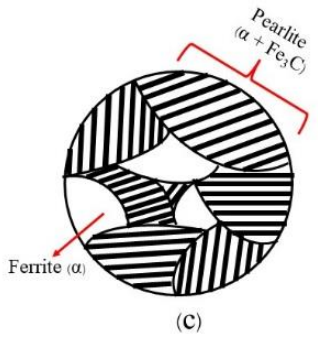

Fig. 1. Microstructure of rails steel (a) Austenitic structure for crossing-nose (b) Pearlitic structure for R260 (c) Pearlitic structure with remaining ferrite for Thermit welded.

2.4 Phased Array Ultrasonic Technique

The OmniScan™ X3 64 Phased Array and TFM Flaw Detector with Advanced Capabilities were used in this study. Numerous wafers comprise a phased array instrument; each can be excited independently. A specialized apparatus propels the probe, transmitting and receiving signals synchronously and independently in each channel. The limitation in defect detection and quantification imposed by conventional ultrasonic wave methods can be reduced to some level by employing an ultrasonic phased array since it depends on the direction of the sound beam [11]. The ultrasonic testing method requires a transducer to produce ultrasonic waves transferred into the examined substance. Subsequently, the waves hit fracture or any other form of imperfection within the substance and undergo reflection towards the transducer. Following that, the waves reflecting are recorded. The recorded signals are used to analyze the imperfections below the material surface. Fig. 2 demonstrates the process by which an ultrasonic transducer examines a crack located under the surface.

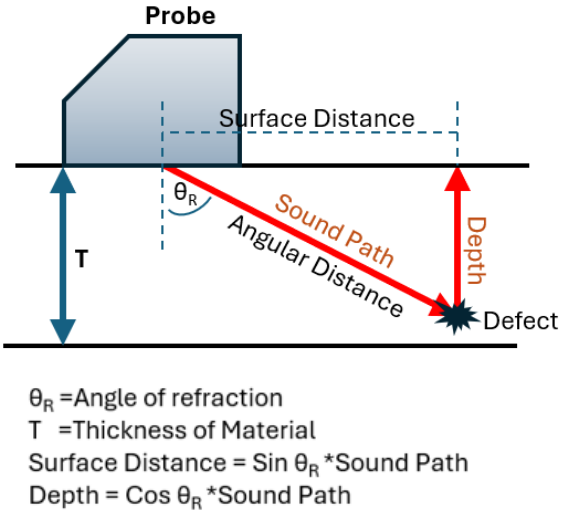

Fig. 2. Illustration of waves travels to detect defects in material.

The parameters of the Phased Array Ultrasonic Inspection used in this study are presented in Table 1.

Table 1. Parameters of the Phased Array Ultrasonic Inspection

Parameter	Value
Detector	Olympus OmniScan™ X3
Probe	SL32-A31
Operating frequency	5.00 MHz
Transmitter voltage	40 V
Receiver gain	29.8 dB
Amplitude threshold	10%
Phased array	32 elements in the bank of 16

2.5 Lab-based testing

OmniScan™ X3 64 Phased Array and TFM Flaw Detector with Advanced Capabilities connected with a cable for the probe head and connected with the probe head is shown in Fig.3. As for testing, the laboratory will calibrate with steel prepared for accurate examination. When calibrating, a couplant was dropped to bring the probe head into contact with the steel. Then, PAUT was used to inspect the rail steel profile cross-section BS100A with artificial cracks, as shown in Fig. 4.

Fig. 3. OmniScan™ X3 64 Phased Array and TFM Flaw Detector with Advanced Capabilities

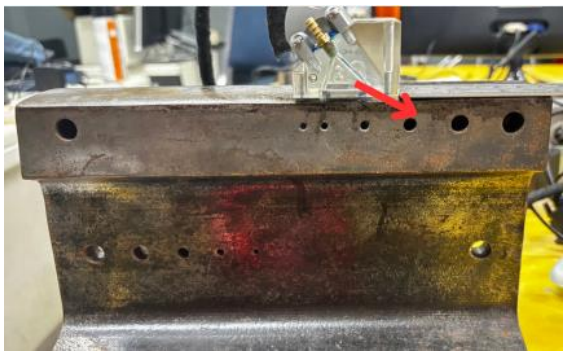

Fig. 4. R260 rail test block with artificial cracks

2.6 On-site testing

On-site testing was done by OmniScan™ X3 64 Phased Array and TFM Flaw Detector with Advanced Capabilities with Probe 32 element in the bank of 16 to check the area of the frog and the thermit welding area, as shown in Fig 5. Use a couplant to apply to the area that needs to be inspected, Fig. 5(a), and use the probe to contact the area that needs to be inspected, as shown in Fig. 5(b).

Fig. 5. PAUT at crossing nose (a) Dropping a couplant on crossing nose surface (b) the PAUT probe head into contact with crossing nose surface

3 Result and discussion

3.1 Artificial crack detection

Laboratory experiments were conducted to prove the focal laws and identify any flaws. The BS100 test block was used to perform the feasibility verification of PAUT. The rail test blocks included drilled holes with different depths and diameters, as seen in Fig. 6. The result is shown in Table 2.

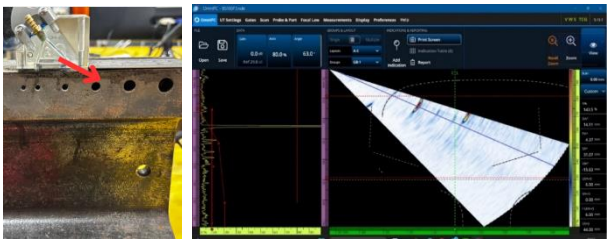

Fig. 6. Laboratory experiments (a) artificial crack for R260 rail test block (b) S-scan for R260 artificial crack

Table 2 shows that PAUT can detect defects at A% equal to 143.5%. A% is the value of the defective Echo (based on A-Scan). The depth from the surface is equal to 14.11 mm, and the distance from the probe to the defect is equal to 31.07 mm. The angle of the signal sent through to the fault is 63˚.

Table 2. The screen results of the phase array tester are all A-scan signals for the R260 rail test block

A%	Depth (mm)	Surface distance (mm)	Angular distance (mm)	Angle (º)
143.5	14.11	4.37	31.07	63

3.2 On-site

OmniScan™ X3 64 Phased Array and TFM Flaw Detector with Advanced Capabilities were used for inspection on-site. Two nose positions and two thermit welds rail joint locations, as shown in Fig.7.

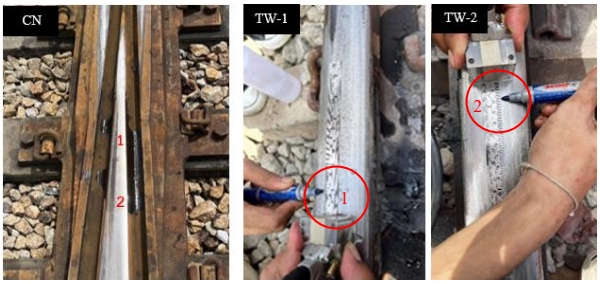

Fig. 7. On-site testing on the crossing nose (CN) and Thermite welded rail joint (TW)

Inspection of the Thermit welded rail joint found two defects; the first has a depth of 14.49 millimeters, and the second has a depth of 31.38 millimeters, while inspection on Crossing Nose two positions has no defects but has color differences. Dark color zones are areas that have received a lot of impact force.

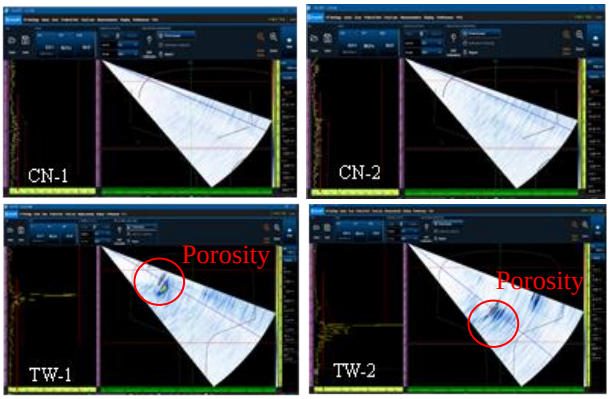

Fig. 8. S-scan images of the crossing nose (CN-1, CN-2) and thermit welded rail joint (TW-1, TW-2)

Table 3. The screen results of the phase array tester are all A-scan signals for the crossing nose and the thermit welded

Positi-on	A%	Depth (mm)	Surface distance (mm)	Angular distance (mm)	Angle (º)
CN-2	12.3	21.41	25.47	52.56	66
CN-1	13.3	16.99	15.53	41.76	66
TW-1	101.0	14.49	2.22	26.88	61
TW-2	119.1	31.38	15.83	52.15	53

Note : CN ; Crossing Nose, TW ; Thermit Welded

Table 3 shows the PAUT inspection of the A-scan section of the crossing nose in two positions and the thermit welded in two positions. It can be seen that the crossing nose in both positions has an echo value that found defect A% equal to 12.3% and 13.3. %, respectively, and the depth from the surface is equal to 21.41 mm and 16.99 mm. The distance from the probe to the defect equals 52.56 mm and 41.76 mm, respectively. Finally, the signal's angle sent through to the defect equals 66˚, which has the same value in both positions.

Results from the PAUT inspection of the A-scan of the Thermit welded in two positions had the echo values found defect A% equal to 101.0% and 119.1%, respectively, and the depth from the surface was equal to 14.49 mm and 31.38 mm, according to the distance from the probe to the defect is 2.22 mm and 15.83 mm. The angle of the signal sent through the defect is 61˚ and 53˚, respectively. It can be seen that the A% of the crossing nose is less than both thermit welded. The welded mechanism detects a defect because the crossing nose has no defect.

Following the standard of the American Railway Engineering and Maintenance of Way Association (AREMA) [13], the defects found in the thermit weld rail joint include porosity, which does not require rejection according to the BART standard [14].

4 Summary

Conducting ultrasonic (UT) inspections on carbon steel (specifically R260 rail steel) is significantly simpler than conducting inspections on austenitic steel. Carbon steel contains a smaller grain structure, resulting in an enhanced ability to transmit ultrasonic waves through the material and a significantly reduced signal-to-noise ratio. On the other hand, Austenitic Steel possesses a significantly larger grain structure, resulting in an increased signal-to-noise ratio.

Through on-site inspection by PAUT, it can be seen that no defects were found in the crossing nose area. However, the characteristics of different color intensities can be seen. Darker areas are more affected by the wheels than light-colored areas. As for the area where the Thermit welded rail joint is, two defects were found ; the first has a depth of 14.49 millimeters, and the second has a depth of 31.38 millimeters. Because Thermit welded is a weld that uses the principle of joint casting, it causes defects in the weld area. According to BART standards [14], if a defect such as crack, shrinkage, or lack of fusion is found, it will be rejected immediately. In this study, only porosity defects were found between the welding line and the rail, so there was no rejection of welds.

Due to its advanced capabilities, investing in PAUT equipment may incur a higher initial expense than conventional ultrasonic (UT) testing systems. Nonetheless, PAUT's superior functionalities lead to quicker, more precise, and more efficient inspections, which can ultimately result in a reduced total cost of ownership.

Acknowledgment

The authors are grateful to the Graduate School and the Department of Mining and Materials Engineering, Faculty of Engineering, Prince of Songkla University, the Railway Engineering Center (PSU-Rail), and the young researcher group under the Thailand Railway Research Network (TRRN) for providing facilities, equipment, and financial support for this project.

References

1. Jessop, C., Ahlström, J., Hammar, L., Fæster, S. and Danielsen, H. K., 3D characterization of rolling contact fatigue crack networks, Wear. **366**, pp. 392-400 (2016). https://doi.org/10.1016/j.wear.2016.06.027
2. Papaelias, M. P., Roberts, C. and Davis, C. L., A review on non-destructive evaluation of rails: state-of-the-art and future development, Proceedings of the Institution of Mechanical Engineers Part F-Journal of Rail and Rapid Transit, **222(4)**, pp. 367-384 (2008). https://doi.org/10.1243/09544097JRRT20
3. Myers, J., Geiger, G., & Poirier, D., Structure and Properties of Thermite Welds in Rails, WELDING J. **61(8)**, pp. 258-268 (1982).
4. Thanapol, J., Manwika, K., Prapas, M., Nichapa, P. and Suhaidee, S., Metallurgy in railway turnout and rail flaw detection techniques. Songklanakarin J. Sci. Technol. **46(2)**, pp. 234-240 (2024)
5. Turgut, P., Research into the correlation between concrete strength and UPV values. NDT. net **12**, no. 12: pp. 1-9 (2004)
6. Lu Chao, Deng Dan, Chen Wensheng, et al., Research on phased array ultrasonic testing for rail pneumatic welding [J], Failure analysis and prevention. **6 (3)**, pp. 139-143 (2011)
7. Chen Xuanmin, Wen Sheng, Study on targeted scan process on rail welds with phased array ultrasonic testing [J], Journal of Railway Science and Engineering. **15 (8)**, pp. 2148-2154 (2018)
8. Curiel-Reyna, E., Contreras, J., Rangel-Ortis, T., Herrera, A., Banos, L., Real, A. d., Rodríguez, M. J. M. and Processes, M., Effect of carbide precipitation on the structure and hardness in the heat-affected zone of Hadfield steel after post-cooling treatments. **23(1)**, pp. 14-20 (2007). https://doi.org/10.1080/10426910701524352
9. Singh, R., Applied welding engineering: processes, codes, and standards, (Butterworth-Heinemann, 2020). https://doi.org/10.1016/b978-0-12-821348-3.00034-3
10. J. Myers, G. Geiger, and D. Poirier, Structure and Properties of Thermite Welds in Rails, WELDING J. vol. **61**, no. 8, pp. 258-268 (1982)
11. G. Kim, M.-K. Seo, Y.-I. Kim, S. Kwon, and K.-B. Kim, Development of phased array ultrasonic system for detecting rail cracks, Sensors and Actuators A: Physical. vol. **311**, p. 112086 (2020). https://doi.org/10.1016/j.sna.2020.112086
12. Fielding, L. C. D., The bainite controversy, Materials Science and Technology, **29(4)**, pp. 383-399 (2013). https://doi.org/10.1179/1743284712Y.0000000157
13. Arema, L. M. D. American railway engineering and maintenance-of-way association. Manual for railway engineering, **2**, pp. 55-57 (2013).
14. BART facilities standards. Standard specification, Running rail section **34 11 25**, pp. 1-36 (2020)